obtained from Eqs. (33) and (36). In addition, the satisfaction of this cusp condition is observed to be independent of the choice of the variational parameter $Z_1$.

ACKNOWLEDGMENT

The authors wish to thank Professor L. B. Mendelsohn for many helpful and stimulating discussions.

*Work supported in part by the Air Force Office of Scientific Research under Grant No. AFOSR 69-1709.

†Taken from the dissertation submitted to the faculty of the Polytechnic Institute of Brooklyn in partial fulfillment of the requirements for the Ph.D. degree (Physics).

‡On leave of absence from the Polytechnic Institute of Brooklyn, Brooklyn, New York.

[1]V. Sahni and J. B. Krieger, Intern. J. Quantum. Chem. Symposium 5, 47 (1971).

[2]J. B. Krieger and V. Sahni, preceding paper, Phys. Rev. A 6, 919 (1972).

[3]H. A. Bethe and R. Jackiw, *Intermediate Quantum Mechanics* (Benjamin, New York, 1969), p. 241.

[4]Y. K. Kim and M. Inokuti, Phys. Rev. 165, 39 (1968). The wave function used by Kim and Inokuti was a three-term analytic Hartree-Fock wave function due to P. S. Bagus and T. L. Gilbert (unpublished) given by $\psi(r_1, r_2) = (4\pi)^{-1}\,\phi(r_1)\,\phi(r_2)$, where $\phi(r) = 4.75657\,e^{-1.450r} - 1.40361re^{-2.641r} - 1.26842re^{-1.723r}$.

[5]R. T. Brown, Phys. Rev. A 1, 1342 (1970); EG&G Technical Reports Nos. EGG-1183-1453 and EGG-1183-1458, 1969 (unpublished).

[6]T. Kato, Commun. Pure Appl. Math. 10, 151 (1957); R. T. Pack and W. B. Brown, J. Chem. Phys. 45, 556 (1966); W. A. Bingel, Z. Naturforsch. 18a, 1249 (1963); E. Steiner, J. Chem. Phys. 39, 2365 (1963).

[7]V. Sahni, Ph.D thesis (Polytechnic Institute of Brooklyn, 1972) (unpublished).

[8]L. M. Shustek and J. B. Krieger, Phys. Rev. A 3, 1253 (1971).

[9]J. C. Y. Chen and A. Dalgarno, Proc. Phys. Soc. (London) 85, 399 (1965).

[10]C. Moller and M. S. Plesset, Phys. Rev. 46, 618 (1934); S. T. Epstein, University of Wisconsin Report No. WIS-TCI-437, 1971 (unpublished).

[11]J. Goodisman and W. Klemperer, J. Chem. Phys. 38, 721 (1963).

[12]L. B. Mendelsohn, Sandia Laboratories Report No. SC-RR-69569, 1969 (unpublished).

[13]C. M. Womack and H. W. Nickerson, Z. Krist. 126, 427 (1968).

[14]A. Papoulis, *The Fourier Integral and its Applications* (McGraw-Hill, New York, 1962), p. 269.

[15]J. N. Silverman and Y. Obata, J. Chem. Phys. 38, 1254 (1963); R. A. Bonham, J. Phys. Chem. 71, 856 (1967).

[16]C. L. Pekeris, Phys. Rev. 115, 1216 (1959).

[17]O. Goscinski and P. Lindner, J. Chem. Phys. 52, 2539 (1970).

[18]H. A. Bethe and E. E. Salpeter, *Quantum Mechanics of One and Two Electron Atoms* (Springer, Berlin, 1957), p. 154.

[19]R. Benesch and V. H. Smith, Intern. J. Quantum Chem. Symposium 5, 35 (1971)

PHYSICAL REVIEW A VOLUME 6, NUMBER 3 SEPTEMBER 1972

# X-Ray Scattering from Liquid Crystals. I. Cholesteryl Nonanoate and Myristate

W. L. McMillan
*Bell Laboratories, Murray Hill, New Jersey* 07974
(Received 2 March 1972)

X-ray scattering intensities from unoriented samples of cholesteryl nonanoate and myristate are reported for several temperatures in the smectic *A*, cholesteric, and isotropic liquid phases. The measured Bragg-scattering intensities from the smectic planes are used to test a recent theoretical model of the smectic *A* phase. Strong pretransition scattering (short-range-order or order-parameter fluctuations) are observed in the cholesteric phase and a Landau theory is constructed to describe this effect.

## I. INTRODUCTION

In his classic study of liquid crystals Friedel[1] differentiated three types of phases—nematic, cholesteric, and smectic. The nematics and cholesterics exhibit orientational order with the long molecular axis oriented preferentially parallel to an axis in space. In cholesterics this preferred axis has a helical twist but from the thermodynamic point of view the two phases are the same. The nematic is just a cholesteric with infinite helical pitch. For the smectics then under study Friedel[1] postulated and Friedel[2] verified a planar structure.

The nematics and cholesterics have been studied intensively for the last few years and the theoretical situation is well advanced. One has a microscopic theory due to Maier and Saupe,[3] a continuum elastic theory[4,5] which has been extended

to a Landau theory[6] describing the nematic-isotropic phase transition and, finally, a hydrodynamic theory[7–9] has been developed. There have been a number of experiments testing various aspects of the theory.

By contrast the smectic phases have received little attention. Herrmann's[10] x-ray photographs exhibited a smectic phase with hexagonal order within the planes and selective miscibility studies[11] have shown the existence of several smectic phases. Recently the microscopic Maier-Saupe theory was extended to the smectic $A$ phase by Kobayashi[12] and by the author.[13] The theory assumed a model intermolecular potential and solved self-consistently for the orientational and (one-dimensional) translational order. From the theory one finds the temperature dependence of the two order parameters

$$\eta = \langle \tfrac{3}{2}\cos^2\theta - \tfrac{1}{2} \rangle \tag{1}$$

describing the orientational order and

$$\tau = \langle \cos(2\pi z/d) \rangle \tag{2}$$

describing the amplitude of the one-dimensional density wave. Here $\theta$ is the angle between the long molecular axis and the $z$ (preferred) axis and $d$ is the interplanar spacing.

The translational order parameter $\tau$ can be measured directly by measuring the x-ray Bragg-scattering intensity vs temperature: $\tau^2 \alpha I_B$. In this way one gets the most direct test of the theoretical model and this was the motivation for the present experimental study. We find that the model intermolecular potential requires some improvement. Early in the experimental work we observed pretransition phenomena in the cholesteric phase and in order to characterize this phenomena we have measured the scattered intensity versus angle in the cholesteric and isotropic liquid phases using monochromatic copper $K\alpha$ radiation. These measurements were performed at twelve temperatures between 56 and 95 °C which covered the smectic $A$, cholesteric, and isotropic liquid ranges for cholesteryl nonanoate and cholesteryl myristate. In addition, in order to determine in detail the temperature dependence of Bragg scattering, the scattering angle was fixed at the Bragg angle and the temperature swept over the same range.

We discuss the pretransition phenomena in terms of a Landau theory of the order-parameter fluctuations. One can calculate the "enhancement factor" of the Landau theory from the microscopic theory and we find it useful to do this. The microscopic theory is not realistic enough to provide the other Landau theory parameters. We find that the experimental data in the cholesteric and isotropic liquid phases can be fit using the Landau theory with the microscopic "enhancement factor." However our data on unoriented samples does not uniquely determine all of the Landau theory parameters and it is desirable to have experiments on oriented samples at higher resolution.

The plan of the paper is as follows. In Sec. II, we discuss the details of the x-ray apparatus and in Sec. III, we present the experimental results. In Sec. IV, we develop the microscopic theory with a modified model potential and calculate the "enhancement factor." In Sec. V, we present the simple Landau theory and calculate the fluctuation contribution to the liquid structure factor. Finally in Sec. VI, we fit the Landau theory to the experimental data in the cholesteric and isotropic liquid phases and compare the microscopic theory with the smectic-phase Bragg-scattered intensity.

## II. APPARATUS

The apparatus is outlined in Fig. 1 and consists of a x-ray source, a monochromator, a regulated hot stage for the sample, a scintillation counter and equipment to control the temperature and scattering angle and to record the scattered intensity. The x-ray source (X) is a conventional GE CA-7H copper x-ray tube with a GE XRD5 power supply with regulated voltage and current (25 kV peak, 20 mA). The collimated beam is monochromatized by a bent LiF crystal (M) and a final collimator limits the angular divergence of the beam. The collimators (C) are 1 mm in diameter and circular and are spaced 22 cm apart giving an angular divergence of 15 min of arc. The primary beam passes through the sample (L) into the beam stop (S). A LiF crystal mounted on the beam stop deflects a portion of the primary beam into scintillation counter (B) to permit continuous monitoring of the incident beam intensity. The scattered beam passes through an annular ring collimator $C'$ with a radius of 1 cm and a slit width of 1 mm and is counted in scintillation counter A. The pulse-height analyzer outputs from channels $A$ and $B$ are fed into a frequency counter operated in the ratio mode whose output is then the ratio of scat-

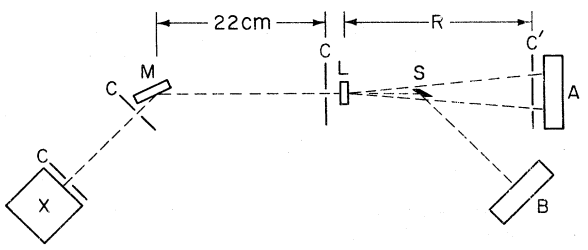


FIG. 1. Sketch of the apparatus which is described in the text. (X) x-ray source; (C) collimators; (M) monochromator crystal; (L) hot stage containing sample; (S) beam stop; (C′) annular ring collimator; (A) and (B) scintillation counters.

tered intensity to transmitted primary beam intensity. Scattered intensities vary from about 10 counts/sec in the isotropic liquid phase to 200 counts/sec in the smectic A phase and the counting time is about 100 sec. The scattering angle is given by $\tan 2\theta = 1\ \mathrm{cm}/R$, where $R$ is the sample to ring collimator distance and the angle is changed by translating the collimator and counter $A$ on an optical bench. The angular range covered is $0.0115 < (\sin\theta)/\lambda < 0.04\ \text{Å}^{-1}$ which is equivalent to a $d$-spacing range of 12.5–43 Å. The interplanar spacings of cholesteryl nonanoate (myristate) are about 27 Å (33 Å). The counter is translated slowly down the optical bench by a servomotor and its position is sensed by a ten-turn potentiometer attached to the gear box.

The hot stage consists of an outer copper can thermally regulated within $\pm 0.2\,^{\circ}\mathrm{C}$ and an inner copper sample holder regulated within $\pm 0.02\,^{\circ}\mathrm{C}$. The temperatures are sensed by thermistors in a bridge circuit. The bridge off balance signals are amplified and used to switch off and on the heater power. The third leg of the bridge contains a motor driven 10-turn potentiometer so that the temperature can be continuously swept. The temperature is swept at $0.05\,^{\circ}\mathrm{C}/\mathrm{min}$ for the data in Figs. 4 and 5. Alternatively a stepping switch can be used to change the resistance in the third leg of the bridge so that data can be taken versus angle at a sequence of fixed temperatures. The sample temperature is measured by a platinum resistance thermometer (in contact with the copper sample holder) which was calibrated in melting ice and in condensing water vapor.

The liquid-crystal sample sits in a 2-mm hole in a 1.6-mm-thick copper block with $\frac{3}{4}$-mil Mylar windows on both sides; Mylar windows are also used on the outer hot stage.

Data are taken in two modes. (i) Fixed temperature, where the temperature is held constant and the counter is translated to change the scattering angle. The scattered beam is counted for about 100 sec (the actual counting time is inversely proportional to the primary beam intensity) and the count and position potentiometer voltage are printed and plotted on an $x$-$y$ recorder. At the end of the angular sweep the temperature is changed by advancing the stepping switch and the sample equilibrates while the counter is returned to its starting position. In this way intensity-vs-angle data are taken automatically for twelve temperatures. (ii) Fixed angle, where the counter is positioned at the average Bragg angle in the smectic $A$ phase and the temperature is swept by the motor-driven potentiometer in the hot-stage bridge. Starting in the isotropic liquid phase the sample is cooled slowly to the lowest desired temperature in the smectic $A$ phase and then heated slowly to the isotropic liquid phase. The sample temperature is measured from the off-balance signal from the platinum resistance thermometer bridge. The scattered intensity and temperature signal are printed and plotted on the $x$-$y$ recorder. Typical data are shown in Figs. 4 and 5.

Cholesteryl nonanoate was obtained from K and K Laboratories and recrystallized three times from $n$-pentyl alcohol. Cholesteryl myristate was obtained from Eastman and recrystallized twice from ethanol and once from $n$-pentyl alcohol. The samples were examined in a polarizing microscope equipped with a Mettler FP5 hot stage. The thermal transitions were observed by differential scanning calorimetry on a Perkin-Elmer DSC-1B. The transition temperatures and heats of transition are given in Table I and agree with results of other workers.[14] The widths of the melting transitions indicate an insoluble impurity content of less than one percent. Commercial samples are known to

TABLE I. Measured transition temperatures (Mettler FP5 hot stage) and transition entropies (DSC 1B) together with the transition entropies and model parameters for models A and B.

| | Cholesteryl nonanoate | Cholesteryl myristate |
|---|---|---|
| Transition temperatures | | |
| solid-liquid crystal | 78.6 | 70.6 |
| smectic-cholesteric | 75.0 | 78.7 |
| cholesteric-isotropic liquid | 91.2 | 83.6 |
| Transition entropies | | |
| smectic-cholesteric (expt.) | $(0.06 \pm 0.04)R_0$ | $(0.43 \pm 0.09)R_0$ |
| cholesteric-isotropic liquid (expt.) | $(0.16 \pm 0.05)R_0$ | $(0.28 \pm 0.07)R_0$ |
| smectic-cholesteric (model A) | $0.74R_0$ | $1.06R_0$ |
| $\alpha$ (model A) | 0.875 | 0.950 |
| smectic-cholesteric (model B) | $0.14R_0$ | $0.47R_0$ |
| $\alpha$ (model B) | 0.415 | 0.4544 |
| $\delta$ (model B) | 0.65 | 0.65 |

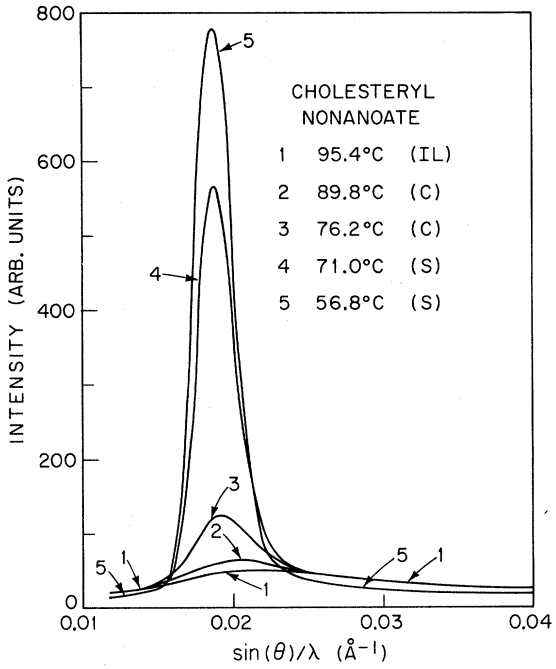


FIG. 2. Measured x-ray scattered intensity per unit solid angle vs scattering angle for cholesteryl nonanoate for five temperatures in the isotropic liquid (IL), cholesteric (C), and smectic *A* (S) phases. To avoid confusion, curves 2, 3, and 4 are plotted only in the region of the peak.

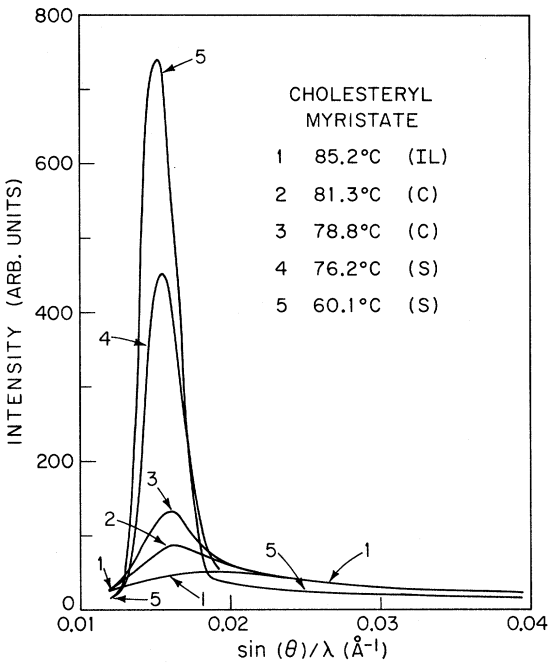


FIG. 3. Measured x-ray scattered intensity per unit solid angle for cholesteryl myristate.

contain homologous impurities which are not removed by recrystallization. The smectic-cholesteric transition has a transition width of 0.1 °C as observed in the intensity of Bragg scattering versus temperature. The materials appear to be as good as those used by other workers in this field and the impurities are believed to have an unimportant effect on the results.

### III. EXPERIMENTAL RESULTS

The measured intensity versus scattering angle for several temperatures are shown in Figs. 2 and 3 for cholesteryl nonanoate and myristate. The data plotted are intensity per unit solid angle and are actual count/(sample-to-counter distance).[2] The intensities are corrected for air absorption of the scattered beam. A background count is taken with an empty sample holder and the background subtracted. The background is primarily due to air scattering of the primary beam and is at most 20% of the measured intensity in the isotropic liquid phase.

The measured intensity versus temperature at the Bragg angle are shown in Figs. 4 and 5 for cholesteryl nonanoate and myristate. In the temperature range shown for the smectic *A* phase the Bragg angle shifts by 1% (2%) for the nonanoate (myristate); positioning the counter at the mean Bragg angle leads to intensity errors of < 1%.

In the isotropic liquid phase we find a broad peak in the scattered intensity at $(\sin\theta)/\lambda = 0.023$

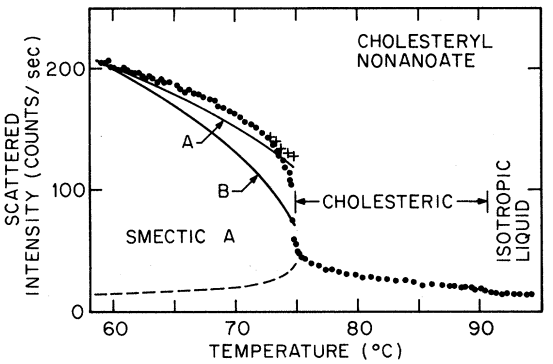


FIG. 4. Measured x-ray scattered intensity vs temperature at the Bragg angle for cholesteryl nonanoate. The points are data taken cooling from the isotropic liquid and the crosses are data taken on the subsequent heating cycle; the crosses are shown only where the heating curve did not reproduce the cooling curve. The dashed line is the calculated diffuse-scattering and fluctuation-scattering contribution. The solid lines labeled A and B are the Bragg scattering plus diffuse and fluctuation scattering calculated from the microscopic theory for model potentials A and B, respectively. The theoretical intensity has been fit to the experimental intensity at the lowest temperature.

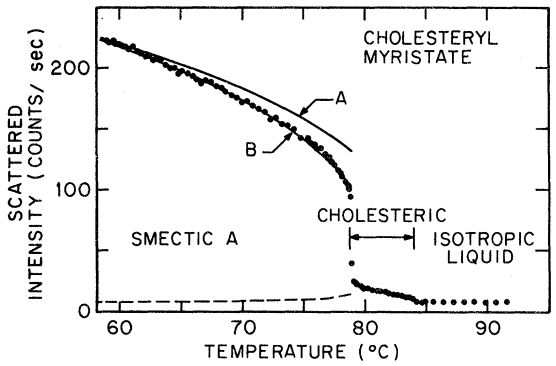


FIG. 5. Measured x-ray scattered intensity vs temperature at the Bragg angle for cholesteryl myristate. The points are data taken cooling from the isotropic liquid which reproduced well on heating. The theoretical curves are labeled as in Fig. 4.

(0.019) $Å^{-1}$ for the nonanoate (myristate). Other workers observe another peak at larger angles which is not studied here. This two-peaked structure is characteristic of excluded volume effects for strongly anisotropic molecules with the small- (large-) angle peak characteristic of the molecular length (width). In the isotropic liquid phase the scattered intensity is insensitive to temperature and the myristate and nonanoate data can be superimposed merely by shifting the horizontal axis.

In the cholesteric phase the small-angle peak grows larger and sharpens up and moves to smaller angle as the temperature is lowered. There is a small but usually detectable jump in the peak intensity at the cholesteric-isotropic phase transition (Figs. 4 and 5). In the neighborhood of the cholesteric-smectic $A$ phase transition the peak intensity increases sharply. Thus we find that the short-range order at angles characteristic of the molecular length increases upon entering the cholesteric phase and continues to increase as the orientational order in the cholesteric phase increases. Then, just before the transition to the smectic $A$ phase, there is a dramatic increase in the short-range order. One can probably differentiate two physical effects here. The first effect is that the short-range order increases as one increases the angular orientation of the long molecules. This effect follows simply from the excluded volume as sketched in Fig. 6. Lining up the long molecular axes makes it more likely to find the molecules end to end (6b). We expect to find this effect in all nematics and cholesterics. The second effect that the short-range order increases sharply just before the transition to the smectic $A$ phase, is clearly a precursor to the smectic $A$ transition and can be labeled "order-parameter fluctuations." Physically because of van der Waals or dipolar forces the central ring structures attract each other and one finds nearly planar regions of increasing size as one approaches the smectic $A$ transition [Fig. 6(c)]. The magnitude of this effect is quite large. The peak intensity in the cholesteric phase near the smectic $A$ transition is a factor of three larger than the peak intensity in the isotropic liquid phase. The present measurements on unoriented samples are an isotropic average. The effects would be much larger for an oriented nematic. Another precursor effect is well known; the cholesteric untwists in the neighborhood of the smectic $A$ transition. One can show from the Landau theory that the order-parameter fluctuations lead to a stiffening of the twist (and bend) elastic constants and thus to an untwisting of the cholesteric helix. Thus the two precursor phenomena are related.

At the transition to the smectic $A$ phase the intensity at the Bragg angle jumps to a large value and the width of the peak reduces to nearly the instrumental resolution. Upon further cooling the Bragg intensity grows and the peak width narrows slightly. In both the cholesteric and smectic $A$ phases the diffuse scattering at angles well away from the Bragg angle decreases as the temperature is lowered. There is a slight shift of the Bragg peak to smaller angles as the temperature is low-

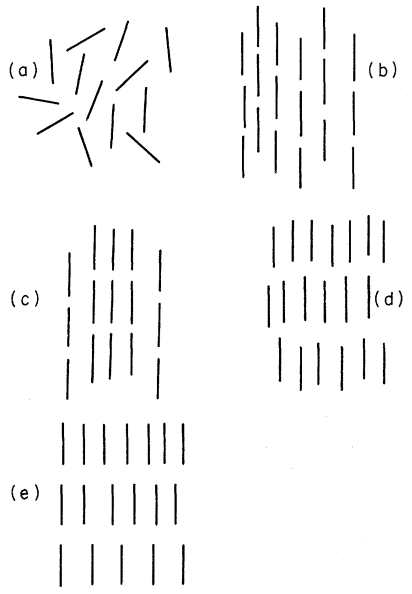


FIG. 6. Sketch of molecular correlations discussed in Sec. III. (a) Isotropic liquid phase with little correlation; (b) nematic phase indicating that parallel alignment of the molecules increases the probability of finding them end to end; (c) nematic phase with central portion in smectic-like planar configuration illustrating pretransition phenomena; (d) smectic $A$ phase with thermal motion of molecules out of planes; (e) perfect smectic $A$ phase.

ered in the smectic $A$ phase. In the nonanoate the shift is 1% on going from 57 to 71 °C and in the myristate the shift is larger, 2% on going from 60 to 76 °C. This shift in $d$ spacing is probably due to a shortening of the average molecular length (due to increased flexibility of the end chains with increasing temperature) although one can think of a number of other possibilities: i.e., a coupling to the orientational or translational order. The principle effect in the smectic $A$ phase, however, is the decreasing intensity of the Bragg peak with increasing temperature (nothing but the Debye–Waller factor) preparatory to the collapse of the planar structure at the transition to the cholesteric phase. This decrease in intensity is due to the thermal motion of the molecules out of the planes and is shown pictorially in Fig. 6(d) compared to the perfectly ordered smectic Fig. 6(e). As this thermal motion increases with increasing temperature the average potential holding the molecules on the planes decreases leading to a further increase of the thermal motion. Thus with increasing temperature the Bragg intensity and the self-consistent potential weaken until the final collapse of the planar structure at the smectic $A$-cholesteric transition. This is the physical basis of the microscopic theory which predicts the temperature dependence of the Bragg scattered intensity. The theory will be compared with the experimental measurements after the theory is further developed in Sec. IV. One expects order-parameter fluctuations in the smectic $A$ phase due to fluctuations in interplanar spacing near $T_{SC}$. This is presumably the cause of the slight increase in linewidth near the transition. However, with the present rather low resolution measurements (the half-width at half-height is 8%) we are unable to resolve the fluctuation scattering from the Bragg scattering in the smectic $A$ phase. We will therefore be forced to use the theory to correct for fluctuation scattering and this will lead to uncertainties in the Bragg-scattered intensity, particularly for the nonanoate.

The absolute intensity in the cholesteric and isotropic liquid phases reproduces well, ±3% from sample to sample. However the absolute intensity of the Bragg peak in the smectic $A$ phase varies from run to run and from sample to sample by 10% or more. The cooling curve accurately reproduces ±2% on heating but subsequent cooling curves can be weaker or stronger. In addition, on wider samples the Bragg intensity varies by ±10% from point to point on the sample. This indicates a weak preferred orientation of the domains in the sample. The temperature variation of the Bragg-scattered intensity reproduces ±2% even though the absolute value may be 30% different. Thus we are able to measure accurately only the temperature dependence of the Bragg intensity and not its absolute magnitude. In addition, for cholesteryl nonanoate there is a weak thermal history effect near the smectic-$A$–cholesteric transition as shown in Fig. 4. This effect is absent in the myristate where the transition entropy is much larger. In the nonanoate the magnitude of the hysteresis is reduced by a factor of two when the cooling rate is reduced by a factor of ten. The temperature sweep is so slow that this is clearly not a thermal lag effect. It is more likely a "strain" effect due to the incomplete untwisting of the cholesteric helix, as one approaches the transition from above.

## IV. MICROSCOPIC THEORY OF SMECTIC $A$ PHASE

The microscopic theory of the smectic $A$ phase has been presented in detail previously[13] and is based on a model intermolecular potential treated within the self-consistent-field approximation. The model was worked out in detail by the author using a two parameter potential, the two parameters being the strength of the potential and its effective range. The model predicts two transition temperatures for the smectic-cholesteric (or nematic) transition $T_{SC}$ and the cholesteric-isotropic liquid transition $T_{CI}$. The two parameters of the model potential can then be determined by fitting the measured transition temperatures and one can compare further predictions of the model with experiment. When used in this way the two-parameter model predicts a universal curve of smectic-cholesteric transition entropy versus ratio of transition temperatures $T_{SC}/T_{CI}$. On comparing this curve with experiment (Fig. 9 of Ref. 13) one finds that the experimental transition entropies for two homologous series are much smaller than predicted. The x-ray measurements reported here indicate that for cholesteryl myristate the order parameter varies more rapidly with temperature in the smectic $A$ phase and exhibits a smaller drop at the phase transition than the theoretical model predicts. The nonanoate data do not agree but are believed to be less reliable. The consistency of the heat-capacity and x-ray data indicate that the theoretical model is predicting a transition which is too strongly first order and that the fault probably lies with the choice of model potential rather than in the method of solution. We therefore feel justified in modifying the model potential to produce better agreement with experiment. The model potential used previously was purely $d$ wave, i.e., proportional to $\frac{3}{2}\cos\theta_{12} - \frac{1}{2}$, where $\theta_{12}$ is the angle between the long axes of the two molecules. This results in a strong coupling between the density-wave order parameter and the orientational order parameter. The density-wave transition is permitted to be second

order by symmetry; however, the strong coupling to the orientational order parameter makes the transition first order where the orientational order parameter varies rapidly with temperature. The transition entropy can be reduced by adding an attractive $s$-wave component to the potential which partially decouples the two order parameters. We thus begin with a model intermolecular potential

$$V_{12}(r_{12},\ \cos\theta_{12}) = -(V_0/N r_0^3 \pi^{3/2}) \times e^{-(r_{12}/r_0)^2}(\tfrac{3}{2}\cos^2\theta_{12} - \tfrac{1}{2} + \delta)\,, \quad (3)$$

where $r_{12}$ is the distance between centers of mass. The self-consistent potential equations are set up and solved as before. Assume a one-particle potential

$$V_1(z,\ \cos\theta) = -V_0[\eta(\tfrac{3}{2}\cos^2\theta - \tfrac{1}{2}) + \alpha\delta\tau\cos(2\pi z/d) + \alpha\sigma\cos(2\pi z/d)(\tfrac{3}{2}\cos^2\theta - \tfrac{1}{2})]\,, \quad (4)$$

where

$$\alpha \equiv 2e^{-(\pi r_0/d)^2} \quad (5)$$

and $d$ is the interplanar spacing. The one-particle distribution function is

$$f_1(z,\ \cos\theta) = \exp[-V_1(z,\ \cos\theta)/kT]\,. \quad (6)$$

Using this distribution function and the intermolecular potential (3) we calculate the average potential felt by one molecule

$$\overline{V}_1(z_1,\ \cos\theta_1) \equiv N\int d^3x_2 d\Omega_2 V_{12}(r_{12},\ \cos\theta_{12}) \times f_1(z_2,\ \cos\theta_2)/\int d^3x_2 d\Omega_2 f_1(z_2,\ \cos\theta_2)\,. \quad (7)$$

We require that this recalculated one-particle potential be equal to the assumed potential (4) and this self-consistency requirement yields the equations for the order parameters. For convenience we add an external potential

$$V_{\text{ext}} = -V_0\alpha\delta\tau_{\text{ext}}\cos(2\pi z/d)\,, \quad (8)$$

then

$$\eta = \langle\tfrac{3}{2}\cos^2\theta - \tfrac{1}{2}\rangle_f\,, \quad (9)$$

$$\tau = \langle\cos(2\pi z/d)\rangle_f + \tau_{\text{ext}}\,, \quad (10)$$

$$\sigma = \langle\cos(2\pi z/d)(\tfrac{3}{2}\cos^2\theta - \tfrac{1}{2})\rangle_f\,, \quad (11)$$

where the thermal average of any one-particle operator $A$ is given by

$$\langle A\rangle_f \equiv \frac{\int d^3x\, d\Omega A(x,\ \Omega) f_1(z,\ \cos\theta)}{\int d^3x\, d\Omega f_1(z,\ \cos\theta)}\,. \quad (12)$$

In (9)–(11), $\eta$ is the orientational order parameter, $\tau$ is the density wave amplitude, and $\sigma$ is a mixed order parameter which is required because the potential couples together the translational and orientational order. The equations are solved numerically by a nonlinear minimization method described previously.[13] One needs the expressions for the entropy $S$ and the internal energy $U$:

$$-TS = NV_0(\eta^2 + \alpha\sigma^2 + \alpha\delta\tau^2) - NkT\ln[(1/d)\int_0^d dz\int_0^1 d(\cos\theta)\, e^{-V_1/kT}]\,, \quad (13)$$

$$U = -\tfrac{1}{2}NV_0(\eta^2 + \alpha\sigma^2 + \alpha\delta\tau^2)\,. \quad (14)$$

For fixed model-potential parameters $V_0$, $r_0$, $\delta$ (and with $\tau_{\text{ext}} = 0$) the equations are solved for the order parameters, the entropy and heat capacity versus temperature. We now have three model-potential parameters and these are fixed by requiring the model to fit the measured transition temperatures, $T_{SC}$ and $T_{CI}$, and the smectic-cholesteric transition entropy. The temperature dependence of the order parameters $\eta$ and $\tau$ and the heat capacity are shown in Figs. 7 and 8 for the model potentials (Table I) appropriate for the nonanoate and myristate.

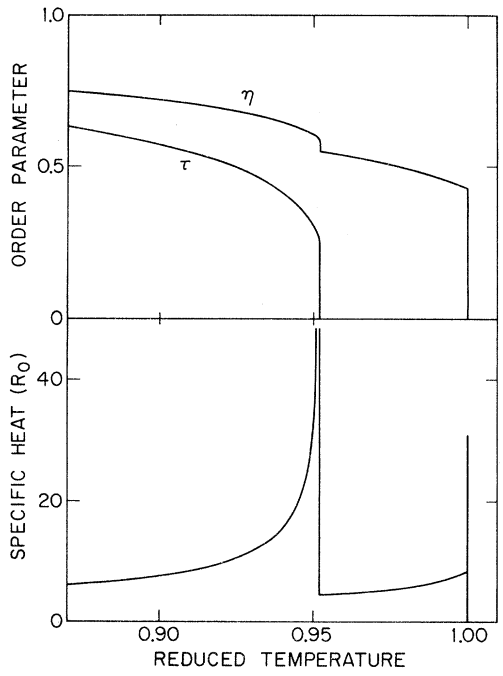


FIG. 7. Order parameters and heat capacity vs reduced temperature ($= T/T_{CI}$) from the microscopic theory (model B) for cholesteryl nonanoate. $\eta$ is the orientational order parameter and $\tau$ is the density wave amplitude.

We turn now to the calculation of the "enhancement factor" from the microscopic model. Within the framework of the model the x-ray scattering is proportional to the liquid-structure factor

$$S_{\vec{q}} \equiv \langle\rho_{\vec{q}}\rho_{-\vec{q}}\rangle\,; \qquad \rho_{\vec{q}} \equiv \sum_i e^{i\vec{q}\cdot\vec{x}_i}\,, \quad (15)$$

where $\vec{x}_i$ is the position of the center of mass of the $i$th molecule. We can compute $S_q$ in the usual

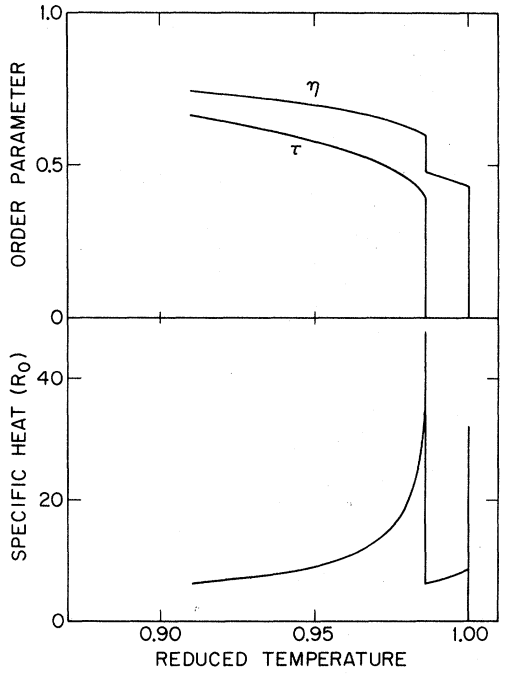


FIG. 8. Order parameters and heat capacity vs reduced temperature from the microscopic theory (model B) for cholesteryl myristate.

way by applying an external field and calculating the response of the system. One can show that

$$S_{\vec{q}} = -\frac{2kT}{V_0\alpha\delta}\frac{\partial\langle\cos qz\rangle}{\partial\tau_{\text{ext}}}. \tag{16}$$

This is useful here only for $q = 2\pi/d$ because the $q$ dependence of the model potential is not realistic. Only this one Fourier component of the model potential has been used in the above thermodynamic calculations. In the cholesteric and isotropic liquid phases one finds a simple expression for the "enhancement factor" $\beta$

$$\beta^{-1} \equiv S_{2\pi/d} = \frac{1+a(\eta^2+b)}{(1-a\delta)(1-ab)-\delta a^2\eta^2}, \tag{17}$$

$$a = V_0\alpha/2kT, \quad b = \langle(\tfrac{3}{2}\cos^2\theta - \tfrac{1}{2})^2\rangle_f.$$

In the smectic $A$ phase $\beta$ is computed numerically by the nonlinear minimization program which solves for the order parameters. The temperature dependence of this enhancement factor is shown in Fig. 11 for the three-parameter model potentials for cholesteryl nonanoate and myristate.

## V. PHENOMENOLOGICAL THEORY OF CHOLESTERIC (NEMATIC) AND ISOTROPIC LIQUID PHASES

X-ray scattering measures the electron density-density correlation function. In the cholesteryl esters the sterol ring has a higher electron density than the parrafin end chains and one can think of the sterol rings as lumps of electron density moving in a paraffin liquid of lower electron density. Although the sterol rings are anisotropic we neglect this and assume an isotropic molecular form factor $f_q$ for the ring system. The scattered intensity is then proportional to $f_q^2\bar{S}_q$, where $\bar{S}_q$ is the isotropically averaged liquid structure factor [$q = 4\pi(\sin\theta)/\lambda$ is the momentum transferred during the scattering event]. In this section we propose a model for $S_q$ including excluded volume effects and order-parameter fluctuation effects.

### A. Excluded Volume Effects

The molecular shape of the cholesteryl esters and of all liquid-crystal molecules is very anisotropic. We assume a cylindrical excluded volume of length $L$ and diameter $D$ with a region of high electron density at the center. We then look at one molecule oriented in the $z$ direction. The centers of neighboring molecules are excluded from a cylinder of length $L+D$ and diameter $2D$ and we assume a uniform distribution outside this cylinder. The anisotropic structure factor is then

$$S_{\vec{q}} = 1 - N\int_{\text{cyl}} e^{i\vec{q}\cdot\vec{r}}d^3r$$

$$= 1 - N\Omega_{\text{cyl}}\frac{\sin[\frac{1}{2}q_\parallel(L+D)]}{q_\parallel[\frac{1}{2}(L+D)]}\frac{J_1(q_\perp D)}{q_\perp D}, \tag{18}$$

where $J_1$ is a Bessel function, $N$ is the particle density, and $\Omega_{\text{cyl}}$ is the cyclindrical volume; we make the usual assumption that $N\Omega_{\text{cyl}} = 1$. Here $q_\parallel$ and $q_\perp$ are the components of momentum transfer along the $z$ axis and perpendicular to it. The anisotropic structure factor is thus approximately zero in a pancake-shaped region

$$|q_\parallel| < 4\pi/(L+D), \quad |q_\perp| < 4\pi/D$$

and exhibits a peak just outside this region. We are interested only in the small-angle region where

$$S_{\vec{q}} \approx 1 - \frac{\sin\frac{1}{2}q_\parallel(L+D)}{\frac{1}{2}q_\parallel(L+D)}. \tag{19}$$

### B. Order-Parameter Fluctuation Effects

In the cholesteric phase near the smectic transition we observe a strong peak in $\bar{S}_q$ near the Bragg angle. Physically this is due to small regions of the material fluctuating into a smectic-like configuration and out again. We can treat these fluctuations phenomenologically using a simplified Landau theory. The order parameter for a one-dimensional density wave is a complex scalar quantity

$$\psi(\vec{x}) = \sum_{\vec{q}}\psi_{\vec{q}}e^{i\vec{q}\cdot\vec{x}}, \tag{20}$$

where the particle density is

$$\rho(\vec{x}) = \rho_0\{1 + \mathrm{Re}[\psi(\vec{x})]\} . \tag{21}$$

One assumes a free energy for a density wave of wavelength $2\pi/q$ and amplitude $\psi_{\vec{q}}$ of the following form:

$$F(\vec{q},\ \psi_{\vec{q}},\ T) = \tfrac{1}{2} N k T A_{\vec{q}} \psi_{\vec{q}}^2 , \tag{22}$$

where $A_{\vec{q}}$ has cylindrical and inversion symmetry and $A_{\vec{q}}$ is a minimum for $\hat{q} = \pm \hat{q}_0 = (2\pi/d)\hat{z}$, that is the free energy is minimum for a density wave with planes perpendicular to the preferred direction (the $\hat{z}$ axis) and with interplanar spacing equal to the observed spacing in the smectic phase. We have taken

$$A_{\vec{q}} = \frac{\beta(T) + \alpha_{\parallel}(|q_{\parallel}| - q_0)^2/q_0^2 + \alpha_{\perp} q_{\perp}^2/q_0^2}{1 - \beta(T)} , \tag{23}$$

where one would normally assume

$$\beta(T) = \beta_0 (T - T_{cr})/T_{cr} . \tag{24}$$

Here $T_{cr}$ is a critical temperature somewhat lower than the first-order transition temperature $T_{SC}$. We will not make use of (24) but will use the values of $\beta$ computed from the microscopic model. The thermodynamic average mean-square amplitude is then

$$\langle \psi_{\vec{q}}^2 \rangle \equiv \frac{\int \psi_{\vec{q}}^2 e^{-F_{\vec{q}}/kT}\, d\psi_{\vec{q}}^2}{e^{-F_{\vec{q}}/kT}\, d\psi_{\vec{q}}^2} = \frac{1}{N A_{\vec{q}}} . \tag{25}$$

The thermodynamic average density-density correlation function is

$$\begin{aligned} \rho_2(\vec{r}_{12}) &= (1/\rho_0)\langle \rho(\vec{r}_1)\rho(\vec{r}_2)\rangle \\ &= \rho_0[1 + \textstyle\sum_{\vec{q}} \langle \psi_{\vec{q}}^2 \rangle \cos(\vec{q}\cdot\vec{r}_{12})] \\ &= \rho_0[1 + \textstyle\sum_{\vec{q}} (1/NA_{\vec{q}}) \cos(\vec{q}\cdot\vec{r}_{12})] . \end{aligned} \tag{26}$$

Including excluded volume effects we have

$$\rho_2(\vec{r}_{12}) = \rho_{ev}(\vec{r}_{12})[1 + \textstyle\sum_{\vec{q}} (1/NA_{\vec{q}}) \cos(\vec{q}\cdot\vec{r}_{12})] . \tag{27}$$

Finally Fourier transforming $\rho_2(\vec{r}_{12})$ we find

$$\begin{aligned} S_{\vec{q}} &= 1 + \int [\rho_2(\vec{r}) - \rho_0]\, e^{-i\vec{q}\cdot\vec{r}}\, d^3r \\ &= S_{\vec{q}}^{ev} + \frac{1}{A_{\vec{q}}} - \sum_{\vec{k}} \left( \frac{1 - S_{\vec{k}-\vec{q}}^{ev}}{N A_{\vec{k}}} \right) . \end{aligned} \tag{28}$$

The first term is the liquid-structure factor with excluded volume effects only. The second term is the order-parameter fluctuation contribution. The third term is a subtraction term which is necessary to make the density-density correlation function zero in the excluded volume region. This term acts to reduce the diffuse scattering well away from the Bragg angle and is essential to permit a quantitative comparison of theory and experiment. Equation (28) holds for a molecule oriented in the $z$ direction; one must average (28) over the angular distribution function which is isotropic for unoriented samples.

## VI. CHOLESTERIC AND ISOTROPIC LIQUID PHASES

### A. Cholesteric and Isotropic Liquid Phases

We now have at hand the theoretical apparatus necessary to interpret the data. There are two types of questions which one would like to have answered. First of all one would like to know whether or not the physical picture of order-parameter fluctuations as described by the Landau theory is qualitatively correct. We will show that the Landau theory appears to work well over a broad temperature range. Second, one would like to be able to determine the parameters of the Landau theory from the data and to test the microscopic model predictions of the enhancement factor $\beta(T)$. We find, however, that there are too many parameters in the theory and not enough information in the data. One cannot uniquely determine all the parameters from the data and we must settle for the more modest goal of finding a physically reasonable set of parameters which are consistent with the data. It turns out that one can fit the nonanoate data using the values of $\beta(T)$ calculated from the microscopic theory; the other parameters are independent of temperature and can be chosen to get a good fit to $I(\theta)$ at several temperatures.

The fitting procedure used is the following. We chose a simple analytic form for the molecular structure factor with two adjustable parameters

$$f_q^2 = f_0^2/(1 + \gamma^2 q^2) . \tag{29}$$

For the excluded volume we chose $L/D = 5$ and $L$ equal to the measured $d$ spacing in the smectic $A$ phase. For the Landau theory parameters we chose $q_0 = 2\pi/d$ and took $\beta(T)$ from the microscopic theory. This left two more parameters $\alpha_{\perp}$ and $\alpha_{\parallel}$ to be adjusted. The particle density was determined from the liquid density ($\approx 1$ g/cm$^3$ estimated from the measured x-ray absorption length) and the molecular weight. We then adjusted the four abailable parameters to fit the nonanoate data in the isotropic liquid phase at $T = 95.5\,^{\circ}$C and in the cholesteric phase at $T = 76.2\,^{\circ}$C. The parameter values are $f_0^2 = 130$ (units of Fig. 9), $\gamma = 0.8/q_0$, $\alpha_{\parallel} = 20$, and $\alpha_{\perp} = 0.5$. The instrumental resolution was folded into the calculated intensity curve. The nonanoate data at intermediate temperatures agreed well with the theory using the appropriate $\beta(T)$ values. The fit for three temperatures is shown in Fig. 9. The values of $\alpha$ are very anisotropic but the anisotropy is not well determined by the data; values of $\alpha_{\parallel}/\alpha_{\perp}$ between 10 and 100 gave an acceptable fit to the data. For smaller values

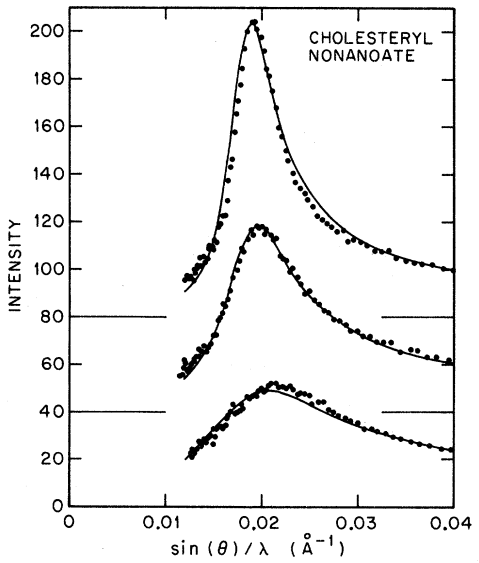


FIG. 9. Scattered intensity vs scattering angle for cholesteryl nonanoate. The lower curve is in the isotropic liquid phase at 95.4 °C, the middle curve is in the cholesteric phase at 85.2 °C and the upper curve is in the cholesteric phase at 76.2 °C. Successive curves are offset vertically by 20 units for clarity. The points are the experimental data and the lines are the Landau theory fit with four adjustable parameters but with $\beta(T)$ computed from the microscopic theory.

of $\alpha_{\parallel}/\alpha_{\perp}$ the theoretical peak becomes too broad and for larger values it becomes too skewed toward large angles. The product $\alpha_{\perp}\alpha_{\parallel}$ and the other two parameters are closely fixed by the data.

We will see below that the microscopic model for the myristate predicts a critical temperature which is too low and consequently the $\beta(T)$ values are a little off. We have therefore fit the myristate data using $f_0^2$, $\gamma$, $\alpha_{\perp}$, and $\alpha_{\parallel}$ given above and adjusting $\beta$ at each temperature to give a good fit. The fit to the data at three temperatures is shown in Fig. 10. The same absolute structure factor was used for the nonanoate and myristate.

We can now make use of the measured intensity at the Bragg angle vs temperature to determine a detailed experimental curve of $\beta(T)$. We computed the intensity at the Bragg angle as a function of $\beta$ using the values of $f_0^2$, $\gamma$, $\alpha_{\perp}$, and $\alpha_{\parallel}$ determined above. Then from the measured intensity at a given temperature (Figs. 4 and 5) and the $I(\beta)$ curve we can read off a value of $\beta$ for that temperature. This analysis of the $I(T)$ data is shown in Fig. 11 for cholesteryl nonanoate and myristate along with the $\beta(T)$ computed from the microscopic theory. Keep in mind that the nonanoate $\beta$ was forced to fit the model $\beta$ at 76.2 °C and in the isotropic liquid phase. The only significant deviation is found in the fact that the microscopic model for the myristate predicts a critical temperature 2.2° below the first-order transition temperature whereas the experimental $\beta(T)$ curve extrapolates to zero at most a few tenths of a degree below the transition temperature.

### B. Smectic *A* Phase

At the transition to the smectic *A* phase the intensity at the Bragg angle jumps abruptly to a large value and continues to increase as the temperature is further decreased. At the transition the width of the peak drops to nearly the instrumental resolution. There are three small effects which occur in the smectic *A* phase: (i) The width of the Bragg peak decreases slightly with decreasing temperature, (ii) the position of the Bragg peak shifts slightly to smaller angles with decreasing temperature, and (iii) the diffuse scattering at angles well away from the Bragg angle decreases with decreasing temperature. The slight increase in linewidth near the transition is probably due to order-parameter fluctuations in the smectic *A* phase. With the present resolution we are unable to resolve the Bragg-scattering and fluctuation contributions. However, we can estimate the fluctuation contribution from the Landau theory using the computed $\beta(T)$ in the smectic *A* phase and the experimental values of the other parameters. The fluctuation

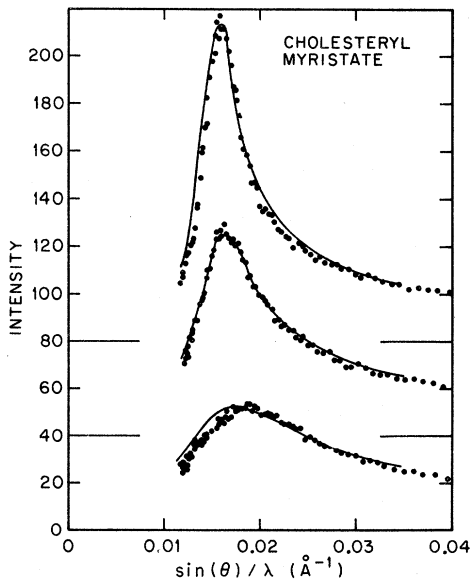


FIG. 10. Scattered intensity vs scattering angle for cholesteryl myristate. The lower curve is in the isotropic liquid phase at 85.2 °C, the middle curve is in the cholesteric phase at 81.3 °C and the upper curve is in the cholesteric phase at 78.8 °C. The points are the experimental data and the lines are the Landau theory fit with one adjustable parameter $\beta(T)$; the other parameters were taken from the nonanoate fit.

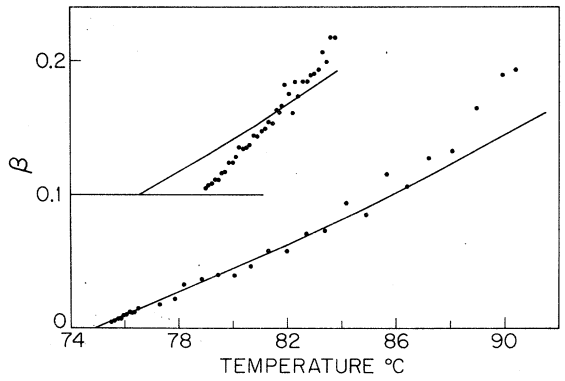


FIG. 11. Enhancement factor $\beta$ vs temperature. The points are experimental values extracted from the data of Figs. 4 and 5 using the Landau theory. The solid lines are the values calculated from the microscopic theory (model B). The lower curve is the data for cholesteryl nonanoate and the upper curve is data for cholesteryl myristate. For the nonanoate the theoretical curve is forced to fit the experimental at 76.2 °C and in the isotropic liquid by the fitting process which determined the Landau theory parameters.

and diffuse scattering contributions to the Bragg-angle scattering are shown in Figs. 4 and 5 as a dashed line.

We are now ready to test the microscopic theory. The Bragg scattering is proportional to the square of the order parameter $\tau$. The proportionality constant is determined by fitting the observed intensity at the lowest measured temperature; there are no other free parameters. The theoretical Bragg-scattering intensities are added to the fluctuation and diffuse-scattering term and plotted in Figs. 4 and 5 for the two model potentials. Model A is the original model with only $d$-wave potential which predicts a too large transition entropy. Model B contains an additional $s$-wave term and has been fit to the transition entropy. The model parameters are given in Table I. The myristate sample behaves exactly as expected. Model A predicts too weak a temperature variation of the scattered intensity and too large a jump at the transition. Model B exhibits excellent agreement with the measured intensity. The fluctuation contribution is small enough to be unimportant. For the nonanoate the story is different. Model A appears to agree with the x-ray data; however, the entropy jump is far too large. Model B predicts a too rapid temperature dependence of the scattered intensity. Here the fluctuation contribution is much more important and errors in its estimation may be partly responsible for the discrepancy. The nonanoate sits almost on the critical point separating the first- and second-order regions in the phase diagram and there may be special problems with the theory here. There are certainly large order-parameter fluctuations. Thus we are unable to assign the discrepancy either to the theory or to the experiment; further work is clearly required.

## VII. CONCLUSIONS

We have presented x-ray intensities versus scattering angle (for monochromatic Cu$K\alpha$ radiation) for several temperatures in the smectic $A$, cholesteric, and isotropic liquid phases of cholesteryl nonanoate and cholesteryl myristate. The motivation for this work was to provide a quantitative test of the microscopic model of the smectic $A$ phase. The x-ray experiment measures the order parameter directly and provides the most detailed test of the theory. It was found desirable to modify the model potential in the theory to improve the agreement with experiment. Even with this improvement in the theory it was found that one sample agreed well with the theory and the second did not. The reason for this discrepancy is not known and it is clearly desirable to have more experimental work on a wider variety of materials.

We have in addition observed short-range-order effects in the cholesteric and isotropic liquid phases and have attempted to provide the theoretical framework necessary to understand these effects. We have presented a simple Landau theory of the order-parameter fluctuations and have calculated the "enhancement factor" from the microscopic theory. The present experiments on unoriented samples are not inconsistent with the Landau theory. However there is insufficient information in the experiment to pin down the Landau theory parameters and we cannot claim to have a rigorous test of the Landau theory. Again further experiments on oriented samples and at higher resolution are desirable.

After this experimental work was completed the author learned of the x-ray experiments of Wendorrf and Price[15] on the same materials. The reader is referred to that paper for details.

## ACKNOWLEDGMENTS

The author has benefited from numerous discussions with many colleagues at Bell Laboratories and from their generosity in the use of equipment.

[1]G. Friedel, Ann. Phys. (Paris) 19, 273 (1922).
[2]E. Friedel, Compt. Rend. 180, 269 (1925).
[3]W. Maier and A. Saupe, Z. Naturforsch. 13A, 564 (1958); 14A, 882 (1959); 15A, 287 (1960).
[4]C. W. Oseen, Trans. Faraday Soc. 29, 883 (1933).
[5]F. C. Frank, Discussions Faraday Soc. 25, 19 (1958).
[6]P. G. de Gennes, Mol. Cryst. Liquid Cryst. 12, 193 (1971).

[7]J. L. Ericksen, Arch. Ratl. Mech. Anal. 4, 231 (1960); 9, 371 (1962).
[8]F. M. Leslie, Quart. J. Mech. Appl. Math. 19, 357 (1966).
[9]Groupe d'Etude des Cristaux Liquides (Orsay), J. Chem. Phys. 51, 816 (1969).
[10]K. Herrmann, Z. Krist. 92, 49 (1935).
[11]H. Sackmann and D. Demus, Mol. Cryst. 2, 81 (1966).
[12]K. Kobayashi, Phys. Letters 31A, 125 (1970); J. Phys. Soc. Japan 29, 101 (1970); Mol. Cryst. Liquid Cryst. 13, 137 (1971).
[13]W. L. McMillan, Phys. Rev. A 4, 1238 (1971).
[14]G. J. Davis and R. S. Porter, Mol. Cryst. Liquid Cryst. 11, 319 (1970).
[15]J. M. Wendorff and F. P. Price (unpublished).

PHYSICAL REVIEW A VOLUME 6, NUMBER 3 SEPTEMBER 1972

# Application of Green's Functions to Radiative Cooperative Effects in Multiatom Systems*

G. Comer Duncan
*Department of Physics, Bowling Green State University, Bowling Green, Ohio* 43403
(Received 14 September 1971)

Spontaneous-radiation processes associated with a number of multiatom systems are studied. Green's-function techniques are used in conjunction with a model of $N$ two-level atoms interacting with a quantized radiation field to investigate the assumption of the independence of the spontaneous-radiation properties of a given atom from the states of the other atoms in the system. It is shown that the natural linewidth of an excited atom in the presence of a deexcited atom is different from that of an isolated excited atom. For interatomic separations smaller than a critical separation, the two-atom system is best considered as a collective unit with regard to its spontaneous-radiation properties. The influence of these "radiative cooperative effects" is studied also for the systems of two initially excited atoms. Also the influence of radiative cooperative effects in the scattering of a photon by a system of two deexcited atoms is studied. It is shown that the frequency distribution of the scattered radiation exhibits a double-peak structure for interatomic separations smaller than $\frac{3}{4}\lambda$. The techniques of Green's functions are then applied to the study of radiative cooperative effects in several many-atom systems. It is shown that within the context of the model certain information is obtained exactly via the Green's-function techniques as applied to the many-atom problems of a single excited atom in the presence of $N \gg 1$ deexcited atoms and the scattering of a photon by a system of $N \gg 1$ deexcited atoms. The necessity of treating many-atom systems from a "collective" point of view is easily seen from our results.

## I. INTRODUCTION

The emission of radiation by a single excited atom is one of the classic problems of quantum electrodynamics. An approximate quantum-mechanical solution was given quite early by Weisskopf and Wigner (WW).[1] The approach of WW has by now become a standard approximation method for computing the lifetime of an excited atomic state, not only for an isolated excited atom but also for systems of many atoms. That is, the usual treatment of the spontaneous radiation emitted by an extended system of atoms is based on the assumption that the individual atoms in the system emit radiation at a rate characteristic of the spontaneous emission rate of a single isolated atom. Consequently, implicit in these treatments is the assumption that the radiation emitted by the individual atoms is independent of the state of the other atoms in the system.

Spontaneous emission of radiation from many-atom systems has been considered by Dicke[2] who recognized the analogy between a system of two-level atoms and a system of spins, and used it to describe a many-atom system interacting through a common radiation field. He showed that under certain conditions the atoms may cooperate in a manner so as to emit radiation at a rate much larger than what would be expected assuming independent emission. Recently, in an impressive work, Rehler and Eberly[3] have reviewed and extended virtually all of the previous results of Dicke and others[4] with regard to the treatment of superradiance. On a much smaller scale, Stephen[5] and Hutchinson and Hameka[6] investigated the problem of a pair of two-level atoms interacting with each other via their common radiation field when one atom is initially excited and the other is deexcited. By extending the methods of the perturbation theory of Heitler[7] to this two-atom system they were able to draw the conclusion that the excited atom radiates at a rate different from that of an isolated atom. In a similar spirit Ernst and Stehle[8] and Ernst[9] "extended" the WW theory of the natural line-